

# Enhanced gamma radiation toward the rotation axis from the immediate vicinity of extremely rotating black holes

Yoogeun Song,<sup>1,2\*</sup> Hung-Yi Pu,<sup>3</sup> Kouichi Hirotani,<sup>3†</sup> Satoki Matsushita,<sup>3</sup>

Albert K. H. Kong,<sup>4</sup> and Hsiang-Kuang Chang<sup>4</sup>

<sup>1</sup> Korea Astronomy and Space Science Institute, Daejeon 305-348, Republic of Korea

<sup>2</sup> University of Science and Technology, Daejeon 305-350, Republic of Korea

<sup>3</sup> Academia Sinica, Institute of Astronomy and Astrophysics (ASIAA), PO Box 23-141, Taipei, Taiwan

<sup>4</sup> Institute of Astronomy, Department of Physics, National Tsing Hua University, No. 101, Section 2, Kuang-Fu Road, Hsinchu, 30013, Taiwan

Accepted XXX. Received YYY; in original form ZZZ

## ABSTRACT

We investigate the acceleration of electrons and positrons by magnetic-field-aligned electric fields in the polar funnel of an accreting black hole (BH). Applying the pulsar outer-gap theory to BH magnetospheres, we find that such a lepton accelerator arises in the immediate vicinity of the event horizon due to frame-dragging, and that their gamma-ray luminosity increases with decreasing accretion rate. Furthermore, we demonstrate that the gamma-ray flux is enhanced along the rotation axis by more than an order of magnitude if the BH spin increases from  $a = 0.90M$  to  $a = 0.9999M$ . As a result, if a ten-solar-mass, almost-maximally rotating BH is located within 3 kpc, when its accretion rate is between 0.005% and 0.01% of the Eddington rate, its high-energy flare becomes detectable with the Fermi/Large Area Telescope, provided that the flare lasts longer than 1.2 months and that we view the source nearly along the rotation axis. In addition, its very-high-energy flux is marginally detectable with the Cherenkov Telescope Array, provided that the flare lasts longer than a night and that our viewing angle is about 45 degrees with respect to the rotation axis.

**Key words:** acceleration of particles – gamma rays: stars – magnetic fields – methods: analytical – stars: black holes

## 1 INTRODUCTION

It is widely accepted that the electromagnetic extraction of the rotational energy of black holes (Blandford & Znajek 1977) is one of the promising mechanisms for powering galactic black hole (BH) binaries and active galactic nuclei. The extracted energy is transported outward in the form of the Poynting and the plasmas' kinetic energy fluxes, and finally dissipated at large distances. However, a portion of this energy can also be dissipated in the vicinity of the BH, if there appears a charge deficit in the magnetosphere in the same manner as in pulsar emission models (Sturrock 1971; Harding et al. 1978; Cheng et al. 1986a; Romani 1996; Hirotani 2013; Takata et al. 2016).

In this context, Beskin et al. (1992) applied the pulsar outer-gap model to BH magnetospheres and pointed out the possibility of an efficient pair-production cascade

near the null-charge surface, where the Goldreich-Julian (GJ) charge density vanishes due to the space-time frame-dragging around a rotating BH. Then Hirotani & Okamoto (1998) demonstrated that the stationary numerical solution obtained from the set of Maxwell-Boltzmann equations is consistent with the gap closure condition (Hirotani et al. 2017, hereafter H17).

In order to consider bright gap emissions, Neronov & Aharonian (2007); Levinson & Rieger (2011); Broderick & Tchekhovskoy (2015), and Hirotani & Pu (2016, hereafter HP16) examined spatially extended gaps, which can be possible in a weak soft photon field. For example, when the mass accretion rate is typically less than 1% of the Eddington rate, the accreting plasmas form a radiatively inefficient accretion flow (RIAF), emitting radio to infrared (i.e., soft) photons via synchrotron process and MeV photons via free-free and inverse-Compton (IC) processes (Ichimaru 1977; Narayan & Yi 1994; Abramowicz et al. 1995; Mahadevan 1997; Manmoto 2000). Under such a low accretion environment, gap-emitted TeV photons do

\* E-mail : ygsong1004@gmail.com

† E-mail : hirotani@tiara.sinica.edu.tw

not efficiently collide with the soft photons, leading to an un-screened, spatially extended gap, which has a much greater electric potential drop than denser soft-photon-field cases.

More recently, [Hirotani et al. \(2016\)](#), hereafter H16) quantified the BH gap model in the two-dimensional poloidal plane, solving the set of the inhomogeneous part of the Maxwell equations, the motion of the created electrons and positrons (which are referred to as leptons in this letter) within the gap, and the radiative transfer equation for the gap-emitted photons, assuming a mono-energetic approximation for the lepton distribution functions. Then H17 considered an inhomogeneous soft photon field to examine the  $\gamma$ -ray emission properties of super-massive BHs (SMBHs), solving the distribution functions of the accelerated leptons explicitly from their Boltzmann equations. In these two works, however, the radial magnetic field strength,  $B^r$ , is assumed to be uniform on the event horizon, because they assumed only moderate BH spins, namely  $a \leq 0.90M$ , where  $M$  is the BH's mass.

However, it was suggested by numerical simulations that the magnetic flux concentrates toward the rotation axis as the BH extremely rotates,  $a \rightarrow M$  ([Komissarov & McKinney 2007](#); [Tchekhovskoy et al. 2010](#)). Indeed, it causes a significant impact on the BH-gap emission. In the present paper, we therefore investigate extremely rotating BHs and demonstrate that their gap emission is strongly beamed toward the rotation axis as  $a \rightarrow M$ .

After briefly describing our methodology in §2, we present our results in §3, and discuss the enhancements from previous works in §4.

## 2 BLACK HOLE GAP MODEL

In this letter, we follow the methodology presented in H17, which is briefly described in §2.1–2.4, incorporating the effect of the magnetic field lines rearranging laterally and concentrating around the axis of rotation (§2.5).

### 2.1 Background geometry

Around a rotating BH, the background geometry is described by the Kerr metric ([Kerr 1963](#)). In the Boyer-Lindquist coordinates ([Boyer & Lindquist 1967](#)), adopting the geometrized unit,  $c = G = 1$ , where  $c$  and  $G$  denote the speed of light and the gravitational constant, respectively, we obtain the following line element,

$$ds^2 = g_{tt}dt^2 + 2g_{t\varphi}dtd\varphi + g_{\varphi\varphi}d\varphi^2 + g_{rr}dr^2 + g_{\theta\theta}d\theta^2, \quad (1)$$

where

$$g_{tt} \equiv -\frac{\Delta - a^2 \sin^2 \theta}{\Sigma}, \quad g_{t\varphi} \equiv -\frac{2Mar \sin^2 \theta}{\Sigma}, \quad (2)$$

$$g_{\varphi\varphi} \equiv \frac{A \sin^2 \theta}{\Sigma}, \quad g_{rr} \equiv \frac{\Sigma}{\Delta}, \quad g_{\theta\theta} \equiv \Sigma; \quad (3)$$

$$\begin{aligned} \Delta &\equiv r^2 - 2Mr + a^2, & \Sigma &\equiv r^2 + a^2 \cos^2 \theta, \\ A &\equiv (r^2 + a^2)^2 - \Delta a^2 \sin^2 \theta. \end{aligned} \quad (4)$$

The horizon radius,  $r_{\text{H}} \equiv M + \sqrt{M^2 - a^2}$ , is obtained by  $\Delta = 0$ , where  $M$  corresponds to the gravitational radius. The spin

parameter becomes  $a = M$  for a maximally rotating BH, and  $a = 0$  for a non-rotating BH.

We assume that the non-corotational potential  $\Phi$  depends on  $t$  and  $\varphi$  only through the form  $\varphi - \Omega_{\text{F}}t$ , where  $\Omega_{\text{F}}$  denotes the magnetic-field-line rotational angular frequency. Under this “stationary” approximation, Gauss’s law gives us the Poisson equation that describes  $\Phi$  in a three dimensional magnetosphere (eq. [15] of H16),

$$-\frac{1}{\sqrt{-g}}\partial_{\mu}\left(\frac{\sqrt{-g}}{\rho_{\text{w}}^2}g^{\mu\nu}g_{\varphi\varphi}\partial_{\nu}\Phi\right) = 4\pi(\rho - \rho_{\text{GJ}}), \quad (5)$$

where the GR GJ charge density is defined as ([Goldreich & Julian 1969](#); [Mestel 1971](#); [Hirotani 2006](#))

$$\rho_{\text{GJ}} \equiv \frac{1}{4\pi\sqrt{-g}}\partial_{\mu}\left[\frac{\sqrt{-g}}{\rho_{\text{w}}^2}g^{\mu\nu}g_{\varphi\varphi}(\Omega_{\text{F}} - \omega)F_{\varphi\nu}\right], \quad (6)$$

where  $\omega \equiv -g_{t\varphi}/g_{\varphi\varphi}$  denotes the frame-dragging frequency at each point. If the real charge density  $\rho$  deviates from the rotationally induced GJ charge density,  $\rho_{\text{GJ}}$ , in some region, equation (5) shows that  $\Phi$  changes as a function of position. Therefore, an acceleration electric field,  $E_{\parallel} = -\partial\Phi/\partial s$ , arises along the magnetic field line, where  $s$  denotes the distance along the magnetic field line. A gap is defined as the spatial region in which  $E_{\parallel}$  is non-vanishing, and appears around the null-charge surface, where  $\rho_{\text{GJ}}$  changes sign (§2.3.2 of HP 16). Because of the frame-dragging effect, the null-charge surface (and hence a gap) appears near the horizon (Fig. 1).

### 2.2 Radiatively inefficient accretion flow

In order to quantify the gap electrodynamics, we need to compute the pair creation rate. In the same way as HP16, H16, and H17, we consider only low-accretion-rate cases and adopt the advection-dominated-accretion flow (ADAF) solution that was obtained analytically by [Mahadevan \(1997\)](#) as a RIAF. We compute the propagation of the ADAF-emitted soft photons (from radio to soft- $\gamma$ -ray energies) in the 3-D rotating magnetosphere, and tabulate their specific intensity at each point in the 2-D poloidal plane, assuming axisymmetry. For details, see §3 of H17. The tabulated specific intensity is used to compute the photon-photon collisions and IC scatterings inside and outside the gap, whose electrodynamics is outlined in the next subsection.

### 2.3 Gap electrodynamics

In the same way (that quantities do not depend on  $\varphi - \Omega_{\text{F}}t$ ) as HP17, we solve the stationary gap solution from the set of the Poisson equation for  $\Phi$ , the equations of motion for the created leptons, and the radiative transfer equation for the emitted photons. Note that the non-uniform, inhomogeneous ADAF photon field at each position in the BH magnetosphere is explicitly taken into account (§2 and Fig. 2 of H17). For the formalism, readers may refer to §4 of H17, for details. The improvement over H17 is that we now take into account the poleward concentration of the magnetic field lines as  $a \rightarrow M$  (with BH mass  $M$ , not gravitational radius) (see Fig. 7 of [Tchekhovskoy et al. 2010](#)), instead of assuming a constant  $B^r$  on  $\theta$ .

## 2.4 Boundary conditions

We impose the same boundary conditions as H17; namely, electrons, positrons, and  $\gamma$ -rays do not penetrate into the gap, except for the ADAF-emitted photons. We assume axisymmetry and solve the gap on the 2-D poloidal plane. We also impose a reflection symmetry with respect to the rotation axis,  $\theta = 0$ , and assume that the gap is bounded from the equatorial, accreting region at  $\theta = 60^\circ$ . Both the inner (i.e., BH-ward) and outer boundaries are solved as free boundaries. Their positions are determined by the following two conditions: (1) the created electric current within the gap is externally given, and (2) a stationary gap solution is obtained by the gap closure condition (§4.2.5 of H17).

## 2.5 Poleward concentration of magnetic field

In HP16 and H16, we computed the radial component of the magnetic field strength as

$$B^r = B_{\text{H}}(2M/r)^2, \quad (7)$$

with a dimensionless accretion rate  $\dot{m}$ , where

$$B_{\text{H}} = 4 \times 10^8 \sqrt{\frac{\dot{m}}{M_1}} G \quad (8)$$

denotes the equipartition magnetic field strength at  $r = 2M$  (Levinson & Rieger 2011), and  $M_1 \equiv M/(10^1 M_\odot)$  for the BH's mass  $M$ . Here,  $M_\odot$  denotes the solar mass. In the present paper, in order to incorporate the  $\theta$  dependence, we compute  $B^r$  with a function  $f_{\text{B}}$  as

$$B^r = f_{\text{B}}(\theta; a) \frac{\partial_\theta A_\varphi^{(0)}}{\Sigma \sin \theta}, \quad (9)$$

where

$$A_\varphi^{(0)} \equiv -(2M)^2 B_{\text{H}} \cos \theta. \quad (10)$$

If we set  $f_{\text{B}} = 1$ , we obtain  $B^r = B_{\text{H}}(2M/r)^2$  for  $r \gg 2M$ . Note that the geometrical factor  $g_{tt} + g_{t\varphi}\Omega_{\text{F}}$  is not multiplied in the right-hand side (Camenzind 1986a,b) to avoid a sign reversal of  $B^r$  near the horizon.

Examining magnetohydrodynamic simulations, Tchekhovskoy et al. (2010) demonstrated that the magnetic field lines progressively bunch up toward the rotation axis as the BH spin increases. For instance, if  $a = 0.5$ ,  $f_{\text{B}}$  takes an almost constant value of 0.29 for  $0^\circ < \theta < 90^\circ$ . However, when  $a = 0.9$ ,  $f_{\text{B}}$  becomes 0.60, 0.58, 0.57, 0.55, 0.52, 0.46, 0.37, and 0.37 at  $\theta = 0^\circ, 5.3^\circ, 10.8^\circ, 16.6^\circ, 23.6^\circ, 34.3^\circ, 63.0^\circ$ , and  $90^\circ$ , respectively. In the extreme case of  $a = 0.9999M$ , they obtained 2.87, 2.62, 2.12, 1.62, 1.25, 0.87, 0.62, and 0.40 at the same  $\theta$ 's. Therefore, at the rotation axis,  $B^r$  becomes 2.1 times stronger if  $a$  increases from  $0.50M$  to  $0.90M$ , and becomes 9.9 times stronger if it increases to  $0.9999M$ . However, at a middle latitude,  $\theta = 23.6^\circ$ ,  $B^r$  becomes only 1.8 to 4.3 times stronger for the same values of  $a$ . This poleward concentration of the magnetic fluxes causes a significant increase of the gap emission along the rotation axis, as will be described in the next section.

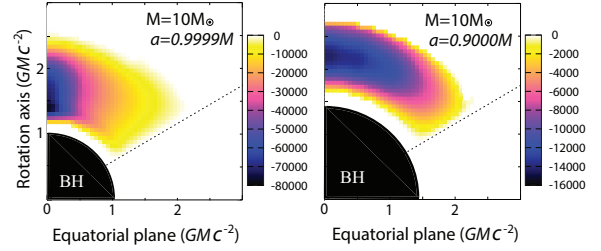


**Figure 1.** Side view of the magnetic-field-aligned electric field,  $E_{\parallel}$  (in statvolt  $\text{cm}^{-1}$ ), exerted in the immediate vicinity of the event horizon. The black hole (BH, the filled circle on the bottom left corner) rotates around the ordinate. Both axes are in the Boyer-Lindquist coordinate and normalized by the gravitational radius of the BH. The thin black dotted line shows the boundary between the polar funnel in which we solve the gap and the equatorial region where the ADAF photons are emitted and illuminates the polar funnel. The dimensionless accretion rate is set to be  $\dot{m} = 1.77 \times 10^{-4}$ . The left panel is for an extremely rotating case with a spin parameter  $a = 0.9999M$ , while the right panel for a rapidly rotating case with  $a = 0.90M$ . It is clear that the gap position can be solved under a free boundary problem (§2.4).

## 3 RESULTS

In the present paper, we adopt  $M = 10M_\odot$  (i.e., stellar-mass) as the BH mass, and compare the results for two different spins,  $a = 0.9999M$  and  $a = 0.90M$ .

### 3.1 The Magnetic-Field-Aligned Electric Field

We begin by considering the distribution of acceleration electric field. In Fig. 1, we present  $E_{\parallel}(r, \theta)$  for  $a = 0.9999M$  and  $a = 0.90M$ . In both panels, the peak of  $|E_{\parallel}|$  appears at the pole,  $\theta = 0^\circ$ . Their maximum values attain  $7.91 \times 10^4 \text{ statvolt cm}^{-1}$  for  $a = 0.9999M$ , and  $1.42 \times 10^4 \text{ statvolt cm}^{-1}$  for  $a = 0.90M$ . Thus,  $E_{\parallel}$  increases about five times from the case of  $a = 0.90M$  to the case of  $a = 0.9999M$ , which is consistent with the increase of  $f_{\text{B}}$  from 0.60 (for  $a = 0.90M$ ) to 2.87 (for  $a = 0.9999M$ ) at  $\theta = 0$ . This enhancement of  $|E_{\parallel}|$  is due to the poleward concentration of the magnetic field lines as  $a \rightarrow M$  (Tchekhovskoy et al. 2010).

### 3.2 Gap Emission versus Colatitudes

Poleward enhancement of  $|E_{\parallel}|$  as  $a \rightarrow M$  results in a poleward enhancement of the outward emission from the gap. In Fig. 2, we compare the resultant  $\gamma$ -ray spectra at five discrete colatitudes, for an extremely rotating case,  $a = 0.9999M$ . The spectra peak in two different  $\gamma$ -ray energies. The lower-energy peak appears in high-energy (HE)  $\gamma$ -rays, between 0.05 GeV and 10 GeV, while the higher-energy peak appears in very-high-energy (VHE)  $\gamma$ -rays, between 0.05 TeV and 1 TeV. The HE emission is due to the curvature process while the VHE one is due to the IC process. It follows that the HE emission becomes most luminous and hardest along the rotation axis (as the solid line shows) and that the VHE emission becomes more luminous and slightly harder along middle latitudes (as the dotted, dash-dot-dot-dotted, and dashed lines show). Since the curvature process dominates the IC process for stellar-mass BHs, the total energy flux integrated between MeV and TeV energies is enhanced

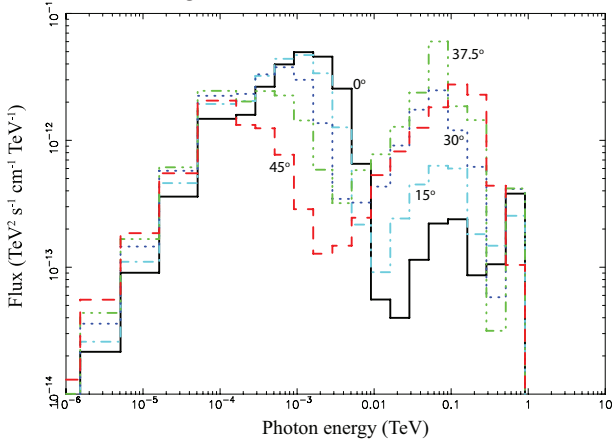


**Figure 2.** Spectral energy distribution (SED) of the gap emission for a stellar-mass BH with  $M = 10M_{\odot}$  and  $a = 0.9999M$ . The distance is assumed to be 3 kpc. The dimensionless accretion rate is chosen to be  $\dot{m} = 7.49 \times 10^{-5}$ . The black solid, cyan dot-dashed, blue dotted, green dash-dot-dot-dotted, and red dashed lines show the SED viewed at the colatitudes  $\theta = 0^{\circ}$ ,  $15^{\circ}$ ,  $30^{\circ}$ ,  $37.5^{\circ}$ , and  $45^{\circ}$ , respectively.

toward the rotation axis for such an extremely rotating BH as  $a = 0.9999M$ . However, such an enhancement is modest for  $a = 0.90M$ , as can be understood from the moderate enhancement of  $B^r$  toward  $\theta = 0^{\circ}$  for  $a = 0.90M$  (§2.5).

### 3.3 Gap emission versus accretion rate

Let us next examine the gap spectrum for  $\theta = 0^{\circ}$  as a function of the dimensionless accretion rate,  $\dot{m}$ . In Fig. 3, we present the SED of gap emission for five discrete values of  $\dot{m}$ , between  $10^{-3}$  and  $5.6 \times 10^{-5}$ . For  $\dot{m} > 10^{-3}$ , we cannot solve the gap accurately, because its longitudinal width becomes too small. On the other hand, for  $\dot{m} < 5.6 \times 10^{-5}$ , the vacuum gap becomes non-stationary and we cannot consider this case in the present stationary analysis. The thin curves on the left show the input ADAF spectra, while the thick lines on the right show the output spectra from the gap. We find that the gap-emitted  $\gamma$ -ray flux increases with decreasing  $\dot{m}$ , because the potential drop in the gap increases with decreasing  $\dot{m}$ .

The spectra peak between 0.1 GeV and 2 GeV for such stellar-mass BHs, because the curvature process dominates the IC one. It is clear that the HE flux lies ten times above the *Fermi*/Large Area Telescope (*Fermi*/LAT) detection limit (the three thin solid curves labeled with “LAT 10 yrs”) <sup>1</sup>, when the accretion rate is  $5.6 \times 10^{-5} \leq \dot{m} \leq 1 \times 10^{-4}$ . Consequently, if a nearby, stellar-mass, extreme Kerr BH ( $M \approx 10M_{\odot}$ ,  $a \approx 0.9999M$ ,  $d < 3$  kpc) spends more than 10% of its time in flaring states (as the green dash-dot-dot-dotted, black solid, and red dashed lines show), the gap emission will be detectable with the *Fermi*/LAT, since the time-averaged flux of the gap emission will appear at ten times lower than the plotted value. Alternatively, if we collect the photons for 1.2 months, the LAT detection limits

will appear at ten times higher value than what are plotted with the thin curves, which means that we can assume a data compilation period of ten years. Therefore, if a BH-gap flare lasts for 1.2 months in a row and if we collect the photons during the same period, we can detect the HE flare with the *Fermi*/LAT.

In order to examine the viewing-angle dependence, in Fig. 4, we present the SED along  $\theta = 45^{\circ}$  for the same case as Fig. 3. It follows that the VHE flux appears a few times above the Cherenkov Telescope Array (CTA) detection limit (the dashed and dotted curves labeled with “CTA 50 hrs”) <sup>2</sup>, when  $5.6 \times 10^{-5} \leq \dot{m} \leq 1 \times 10^{-4}$ . Hence, if a nearby, stellar-mass, extreme Kerr BH ( $M \approx 10M_{\odot}$ ,  $a \approx 0.9999M$ ,  $d < 3$  kpc) experiences a VHE flare (as the green dash-dot-dot-dotted, black solid, and red dashed lines show), and if we view the source at  $\theta \approx 45^{\circ}$ , the gap emission may be marginally detectable with a one-night observation by using the CTA.

Now, let us consider a slower spin,  $a = 0.90M$ . In Fig. 5, we present the SED along  $\theta = 0^{\circ}$ . Since solutions can be found only for  $\dot{m} \geq 1.77 \times 10^{-4}$ , we only plot the cases of  $\dot{m} = 10^{-3.0}$ ,  $10^{-3.5}$ , and  $10^{-3.75}$  as the cyan dash-dotted, blue dotted, and black solid lines. Comparing with the  $a = 0.9999M$  case (i.e., Fig. 3), we find that the  $\gamma$ -ray flux decreases more than an order of magnitude. However, if  $B^r$  were constant on the horizon, as assumed in HP16, H16, and H17, the results still do not change very much between  $a = 0.90M$  and  $a = 0.9999M$ . As a consequence, we can conclude that the poleward enhancement of  $B^r$  as  $a \rightarrow M$  plays a pivotal role in the prominent increase of the BH-gap  $\gamma$ -radiation for an extremely rotating Kerr BH.

## 4 SUMMARY AND DISCUSSION

To summarise, we investigated how the BH gap emission is influenced by the lateral concentration of the magnetic field lines toward the rotation axis,  $\theta = 0^{\circ}$ , as the BH spin approaches its maximum value,  $a \rightarrow M$ . For a stellar-mass BH, the gap shows an enhanced high-energy  $\gamma$ -radiation along the rotation axis, when the dimensionless accretion becomes  $5 \times 10^{-5} < \dot{m} < 10^{-4}$ . If a nearby, extremely rotating, stellar-mass BH experiences such a flare, its gap emission will be detectable with the *Fermi*/LAT, provided that we view the BH nearly along the rotation axis.

Actually, it is not very clear that if an astrophysical BH can be spun up to the near-maximum value,  $a = 0.9999M$ . For instance, such a BH may preferentially capture negative angular momentum photons radiated from the accreting plasmas to spin down to the canonical value,  $a = 0.998M$  (Bardeen 1970; Thorne 1974). In this letter, we adopted such a large value as  $a = 0.9999M$  in order to demonstrate the extreme case. More moderate cases (e.g.,  $a = 0.99M$ ) can be qualitatively interpolated from the two cases we have considered,  $a = 0.90M$  and  $a = 0.9999M$ . If  $a \approx M$ , positive-angular-momentum plasmas will not accrete onto the horizon, whatever  $\dot{m}$  may be small. Nevertheless, the plasmas will be ejected from the equatorial ergosphere as an outflow without penetrating in the polar regions,  $\theta \ll 1$ . Therefore,

<sup>1</sup> [https://www.slac.stanford.edu/exp/glast/groups/canda/lat\\_Performance.htm](https://www.slac.stanford.edu/exp/glast/groups/canda/lat_Performance.htm)

<sup>2</sup> [https://portal.cta-observatory.org/CTA\\_Observatory/performance/SitePages/Home.aspx](https://portal.cta-observatory.org/CTA_Observatory/performance/SitePages/Home.aspx)



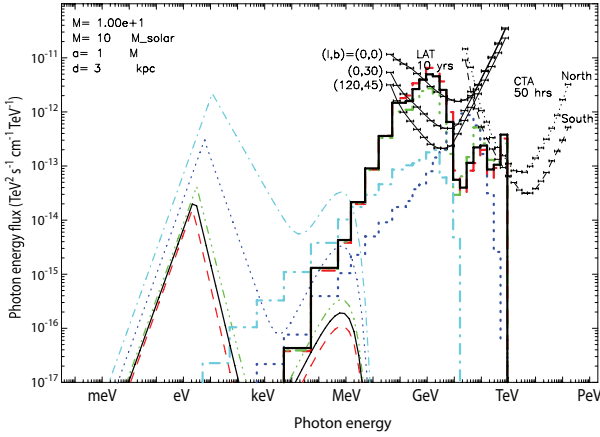


**Figure 3.** SED of gap emission along the rotation axis,  $\theta = 0^\circ$ , for  $M = 10M_\odot$  and  $a = 0.9999M$ . The distance is assumed to be 3 kpc. The cyan dash-dotted, blue dotted, green dash-dot-dot-dotted, black solid, and red dashed lines correspond to the dimension accretion rates,  $\dot{m} = 10^{-3.00}$ ,  $10^{-3.50}$ ,  $10^{-4.00}$ ,  $10^{-4.125}$ , and  $10^{-4.25}$ , respectively. Thus, the black solid line represents the same case as the black solid line of Fig. 2. The three thin curves in the top right part show the detection limit with the *Fermi*/LAT with ten-year observations at galactic longitude  $l$  and latitude  $b$  as designated. The dashed and dotted curves in the top right part show the Cherenkov Telescope Array detection limit after a 50-hour observation for the southern and northern sources, respectively.

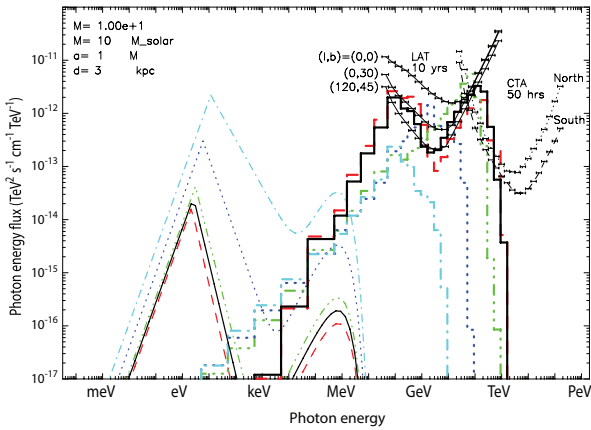


**Figure 4.** SED of gap emission along a middle latitude,  $\theta = 45^\circ$ , for  $M = 10M_\odot$  and  $a = 0.9999M$ . The distance is assumed to be 3 kpc. The lines correspond to the same  $\dot{m}$ 's as in Fig. 3.

in the present argument, it is not essential as to whether or not the plasmas plunge onto the horizon; it is necessary only to form the horizon-penetrating magnetic field.

The poleward enhancement of the  $\gamma$ -ray flux as  $a \rightarrow M$ , indeed, is unaltered if we adopt different BH masses. This is because the magnetic field lines concentrate toward the rotation axis as  $a \rightarrow M$ , irrespective of the BH mass (Tchekhovskoy et al. 2010). However, as the BH mass increases, the IC process dominates the curvature process, leading to a poleward enhancement of VHE radiation for SMBHs, which is to be investigated in a separate paper.

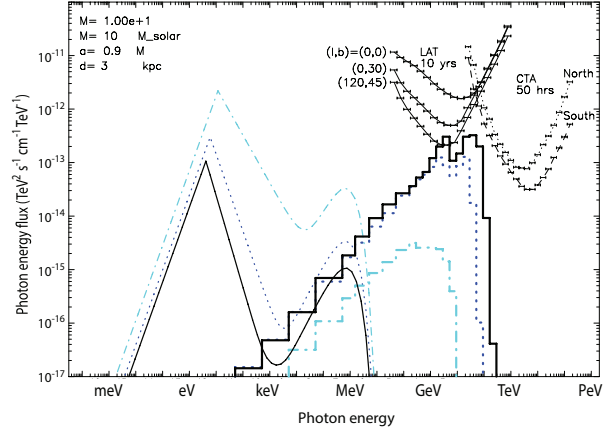


**Figure 5.** SED of gap emission along the rotation axis,  $\theta = 0^\circ$ , for  $M = 10M_\odot$  and  $a = 0.90M$ . The distance is assumed to be 3 kpc. The cyan dash-dotted, blue dotted, and black solid lines corresponds to the dimension accretion rates,  $\dot{m} = 10^{-3.00}$ ,  $10^{-3.50}$ , and  $10^{-3.75}$ , respectively.

## ACKNOWLEDGEMENTS

One of the authors (K. H.) is indebted to Dr. T. Y. Saito for valuable discussion on the CTA sensitivity. This work is supported by the Theoretical Institute for Advanced Research in Astrophysics (TIARA) operated under Academia Sinica, and by the Ministry of Science and Technology of the Republic of China (Taiwan) through grants 103-2628-M-007-003-MY3, 105-2112-M-007-033-MY2, 105-2112-M-007-002, 103-2112-M-001-032-MY3.

## REFERENCES

- Abramowicz M., Chen X., Kato S., Lasota J. P., Regev O., 1995, *ApJ*, 438, L37
- Bardeen J. M., 1970, *Nature*, 226, 64
- Beskin V. S., Istomin Ya. N., Par'ev V. I., 1992, *Sov. Astron.*, 36(6), 642
- Blanford R. D., Znajek R. L., 1977, *MNRAS*, 179, 433
- Boyer R. H., Lindquist R. W., 1967, *J. Math. Phys.*, 265, 281
- Broderick A. E., Tchekhovskoy A., 2015, *ApJ*, 809, 97
- Cheng K. S., Ho C., Ruderman M., 1986, *ApJ*, 300, 500
- Camenzind M. A., 1986a, *A&A*, 156, 137
- Camenzind M. A., 1986b, *A&A*, 162, 32
- Goldreich P., Julian W. H., 1969, *ApJ*, 157, 869
- Harding A. K., Tademaru E., Esposito L. S., 1978, *ApJ*, 225, 226
- Hirovani K., Okamoto I., 1998, *ApJ*, 497, 563
- Hirovani K., 2006, *MPLA*, 21, 1319
- Hirovani K., 2013, *ApJ*, 766, 98
- Hirovani K., Pu H.-Y., 2016, *ApJ*, 818, 50 (HP16)
- Hirovani K., Pu H.-Y., Lin L. C.-C., Chang H.-K., Inoue M., Kong A. K. H., Matsushita S., Tam P.-H. T., 2016, *ApJ*, 818, 50 (H16)
- Hirovani K., Pu H.-Y., Lin L. C.-C., Kong A. K. H., Matsushita S., Asada K., Chang H.-K., Tam P.-H. T., 2017, *ApJ*, in press (H17)
- Ichimaru S., 1977, *ApJ*, 214, 840
- Kerr R. P., 1963, *Phys. Rev. Lett.*, 11, 237
- Komissarov S. S., McKinney J. C., 2007, *MNRAS*, 377, L49
- Levinson A., Rieger F., 2011, *ApJ*, 730, 123
- Mahadevan R., 1997, *ApJ*, 477, 585
- Manmoto T., 2000, *ApJ*, 534, 734
- Mestel L., 1971, *Nature*, 233, 149
- Narayan R., Yi I., 1994, *ApJ*, 428, L13

- Neronov A., Aharonian F. A., 2007, *ApJ*, 671, 85  
Romani R. W., 1996, *ApJ*, 470, 469  
Sturrock P. A., 1971, *ApJ*, 164, 529  
Takata J., Ng C. W., Cheng K. S., 2016, *MNRAS*, 455, 4249  
Tchekhovskoy A., Narayan R., McKinney J. C., 2010, *ApJ*, 711,  
50  
Thorne K. S., 1974, *ApJ*, 191, 507

This paper has been typeset from a  $\text{\TeX}/\text{\LaTeX}$  file prepared by the author.